Dynamical structures of a photorefractive oscillator

J. Malos,* M. Vaupel, K. Staliunas, and C. O. Weiss
Physikalisch-Technische Bundesanstalt, D-38116 Braunschweig, Germany
(Received 22 March 1995; revised manuscript received 13 November 1995)

Using a photorefractive oscillator (PRO) with a stable resonator, we investigate patterns produced from the transverse mode families of order 0–3. The phenomena observed include vortices which move along circular or spiral trajectories and vortices which periodically change the sign of their topological charge. In addition, we observe behavior which is unlike that expected for lasers, despite the established analogy between the laser and the PRO. This includes pulsing of mode patterns which are otherwise expected to be stable, and also stable rotation of Gauss-Laguerre mode patterns. These effects indicate a much stronger self-focusing in the PRO than in lasers.

PACS number(s): 42.65.Sf, 42.55.−f, 42.65.Hw

I. INTRODUCTION

It has recently become apparent that laser physics is closely related with fluid dynamics [1,2]. In lasers, however, the typical time scale is nanoseconds so that the dynamics of patterns are practically inaccessible to observation. It is therefore fortunate that photorefractive oscillators, with their slow dynamics brought about by an extremely narrow gain line with enormous frequency pulling, can be shown to correspond to lasers to class A when operated not too far above threshold [3]. Consequently, they allow investigation of laser dynamics on a time scale convenient for recording.

We report the observed dynamics of laserlike patterns which contain vortices that move in gradients of the background field corresponding to the hydrodynamic analogy of lasers [2]. Dynamics which are not expected from lasers, such as pulsing of otherwise stable patterns and rotating Gauss-Laguerre mode patterns, point to differences between lasers and photorefractive oscillators. These may stem from a more pronounced self-focusing of the active medium, as is expected for photorefractive oscillators higher above threshold.

The experimental setup is shown in Fig. 1 and is essentially as described in [5]. A ring resonator of perimeter 2 m was used with an even number of mirrors. The resonator consists of two plane dielectric mirrors $M1$ and $M3$, polarizing beam splitters (PBS), a BSO crystal (length: 10 mm; width: 5×5 mm^2) as the active medium, plane mirrors ($M1$ and $M2$), both movable by a piezo, two lenses ($L1$ and $L2$) to select the number of transverse modes per free spectral range (approximately four in these experiments), and an iris used to control the losses of the modes. The general field is polarized perpendicular relative to the resonator plane.

To reproducibly excite certain transverse mode families, the resonator length is actively stabilized. A reference beam (part of the pump radiation) is horizontally polarized and propagates counter to the generated field. This is used together with modulation of the resonator length via a piezo on mirror $M1$. The changes in transition of the TEM_{00} resonance due to the modulation are phase-sensitively detected to stabilize the resonator length by the usual feedback technique. The resonator is not absolutely stabilized in length but rather with reference to the pump radiation since the radiation generated is offset by only about 1 Hz from the pump frequency. The short path length between the PBS's including the crystal is not stabilized. However, fluctuations between the two paths are kept to a minimum by the following arrangements: the small ratio of this path length to the total round-trip length, the symmetric setup of both paths, mounting of the PBS's and crystal on an invar plate, and shielding from air currents. This limits the fluctuations to the order of 100 kHz/min, which is very small compared to the resonator mode widths of ~30 MHz.

Transverse mode selection was achieved by moving the mirror $M2$ with a piezo. This change in resonator length is not compensated by the active stabilization but moves the mode frequencies relative to the ''gain line'' of the crystal.

For optical amplification in the resonator, the BSO crystal is pumped through one of the PBS's by an argon-ion laser ($\lambda=514$ nm) with an irradiance of about 3 mW/cm^2. The

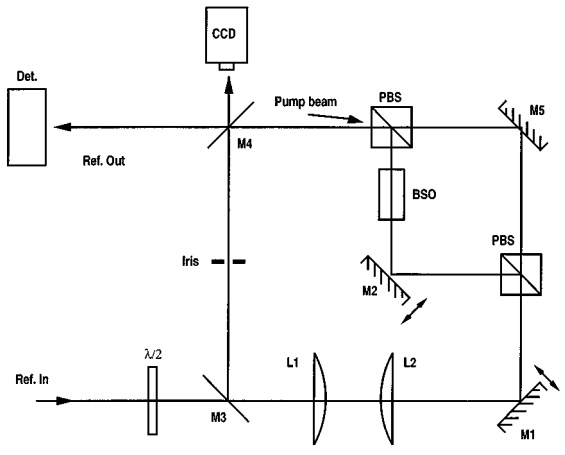

FIG. 1. Experimental setup. The active resonator is formed by four mirrors $M1-M4$ and the (active) BSO crystal. PBS: polarizing beam splitter. The resonator formed by $M1$, $M3$, $M4$, $M5$ has high finesse and is thus suitable for resonator length stabilization. The reference signal is provided by part of the pump radiation with polarization perpendicular to pump and generated field.

*Permanent address: Physics Department, The University of Queensland, Brisbane, Australia.

pump beam propagates at an angle of approximately 0.8° to the direction of the generated field for optimum amplification. The pump beam and generated beam intersect in the 110 plane of the crystal and the field falls off between the 001 surfaces of the crystal, which is the usual geometry. The whole crystal is uniformly illuminated so that the intensity variation across the crystal is less than 1%. To achieve this, the BSO crystal is located at a distance of only 1 cm from the PBS. Care was taken to ensure perfect rotational symmetry of the system because asymmetries can induce unwanted dynamics (e.g., astigmatism, which lifts the frequency degeneracy between perpendicularly oriented patterns). Astigmatism is absent in the resonator because only plane mirrors are used and Brewster surfaces are avoided. The asymmetry introduced by imperfect pump beam alignment was controlled by adjusting its direction so that the Gauss-Hermite TEM_{01} and TEM_{10} mode emission was perfectly quadrature phase locked to form a perfectly round TEM_{01}^{*} Gauss-Laguerre emission pattern. Other tests for rotational symmetry of the resonator included the free rotation of patterns (see below). The resonator uses spherical optics in the stable regime. Thus motion of patterns is mostly angular. The last requirement for gain is a dc voltage on the crystal (5–5.5 kV), because BSO is a drift-type photorefractive material [4]. A portion (10%) of the generated field is coupled out and recorded by a charge-coupled device (CCD) camera.

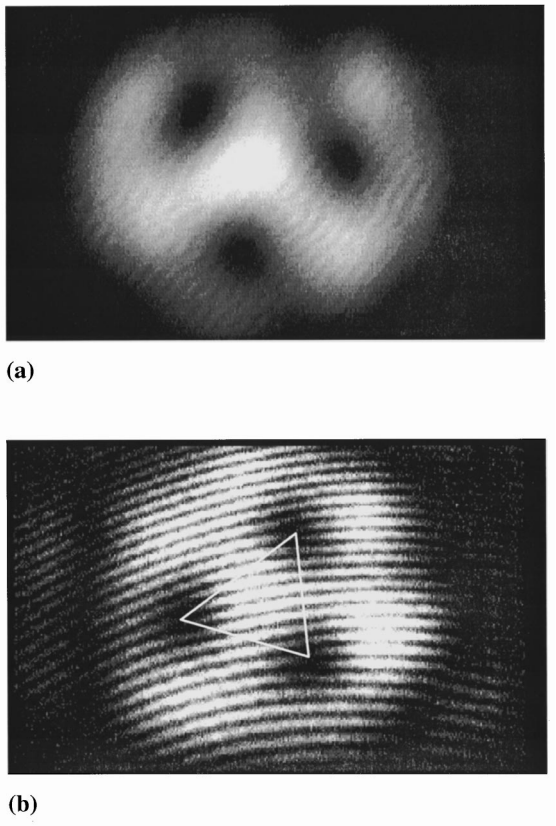

FIG. 2. (a) Single video frame taken from the motion of three circling vortices. (b) An interferogram clearly showing the presence of three vortices of the same helicity as dislocations in the fringe pattern. The triangle indicates the measurement of the distance between vortices and, consequently, circling radius.

II. CIRCLING VORTICES (MODE FAMILIES 0, 1, AND 3)

Recently it has been found that in stable spherical resonators one prominent type of dynamics is motion of one or several vortices [5] on a circular trajectory around the laser axis. This motion may be understood in terms of simultaneous transverse mode emission in different orders or alternatively in the hydrodynamics analogy, as the combined action of buoyancy and Magnus drift [2].

Figure 2 shows the case of three vortices circling around the optical axis, in a snapshot. The light emitted from the photorefractive oscillator (PRO) can be superposed with part of the pump light. The interference pattern thus created shows that all the dislocations of the fringe pattern (''forks'') point to the right. This means that all three vortices have the same helicity.

In a mode picture, the movement of the vortices on a circle is due to the difference in frequency of the two constituent active modes. The vortex trajectory radius is a function of the amplitude ratio of the two. Consequently, by tuning the PRO, the trajectory circle radius may be expected to change [6].

To make such a measurement, one has to take into account that ''active modes'' are far from being rigid entities but are more nearly like softly confined fluids so that they are easily perturbed. A circling vortex pattern emitted by a laser is thus only under very ideal conditions close to the interference of the two passive resonator modes. Consequently, in general the motion of vortices is not on circles, but rather on noncircular contours, even with careful alignment. To average such imperfection, instead of the radius of the trajectory circle, the triangle shown in Fig. 2 was measured and the side lengths averaged. Figure 3 shows the results of such a measurement. It was found that the tuning of the resonator suffered from all imperfections of the tuning piezo element, such as hysteresis and creep. Tuning was therefore done by tilting a glass plate in the reference path of the resonator electromechanically. Figure 3 shows that tuning of about $\frac{1}{3}$ of the spacing between the $q=0$ and 3 family changes the radius of the circle of the trajectory by about $\frac{1}{4}$ of the mode radius.

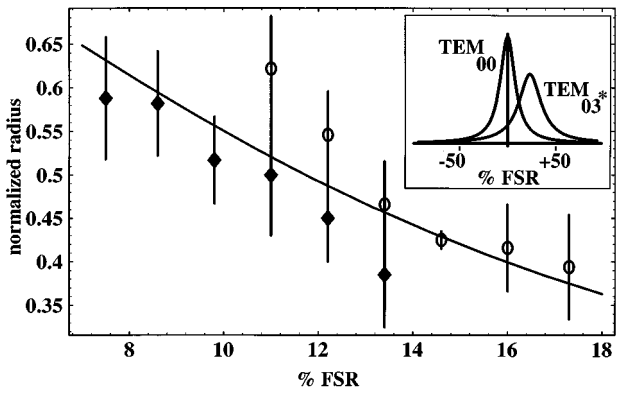

FIG. 3. Vortex circling radius (normalized to the mode radius) versus resonator detuning (percentage of free spectral range). Points show the experimental results for two separate measurements. The solid line is the variation of the vortex radial position (via simple interference of Gaussian and charge 3 doughnut mode) calculated as a function of detuning (see inset).

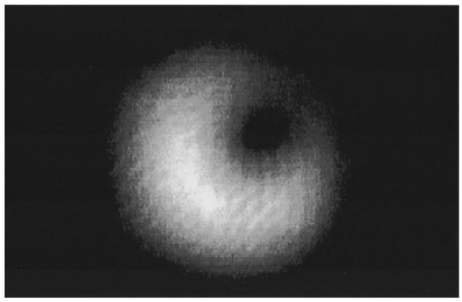

FIG. 4. Single video frame taken from the motion of one vortex circling about the laser optical axis.

For comparison, using the linewidths and the spacing of the $q=0$ and 3 mode families determined from a transmission measurement on the resonator, a rough estimate can be made of the radius of the vortex trajectory as a function of detuning. Assuming that the generated fields are proportional to the amplitude of the passive modes at the frequencies generated (see inset, Fig. 3), the solid line in Fig. 3 is obtained which agrees well with the measurements, considering that the calculation neglects pump threshold and gain saturation. Consequently, the circling of the vortices can be reasonably understood in terms of the linear resonator properties and the material frequency pulling.

A further case of circling vortices arises when the gain line lies between the $q=0$ and 1 mode families of the resonator. In this case only one vortex circles about the laser axis (on the condition that the laser shows no residual astigmatism, e.g., due to imperfect alignment). Figure 4 shows a snapshot of this pattern. Here the trajectory circle of the vortex is about half of the mode radius.

One may ask how the transition from the emission of a field, which contains no vortex, to a field which contains a vortex comes about. Naively, if one ascribes to the vortex solitonlike properties [7], during this transition a vortex could be expected to move in from infinity and settle onto a symmetry point of the field. This transition has been realized by tuning the PRO to TEM_{00} emission and then abruptly changing to the frequency of the $q=1$ mode family (via a voltage step on the tuning element). The transition evolves in the way expected. From the moment that the vortex is observable against the background light it appears as an object not changing its shape, in a fashion similar to a particle or soliton. It moves on a spiral-shaped trajectory from infinity to the optical axis. Figure 5(a) shows the measured trajectory, when switching the resonator frequency from mode family $q=0$ to 1. A spiral is clearly apparent. Figure 5(b) shows the opposite case of tuning from the $q=1$ family to the $q=0$ family. In Figs. 5(a) and 5(b), points indicate vortex positions equidistant in time. From this, the slowing of the motion near the beam center and the acceleration in the outer parts of the beam can be seen. It was generally found that when spiraling outward, the radial component of the velocity was larger than for inward spiraling.

The sizes of the intensity contours are given in Fig. 5. The small contour corresponds to the TEM_{00} mode and the large contour to the TEM_{01}^{*}. The ratio of the diameters of the empty resonator modes is $\sqrt{2}$. However, the larger ratio of the active modes observed here may be due to self-focusing,

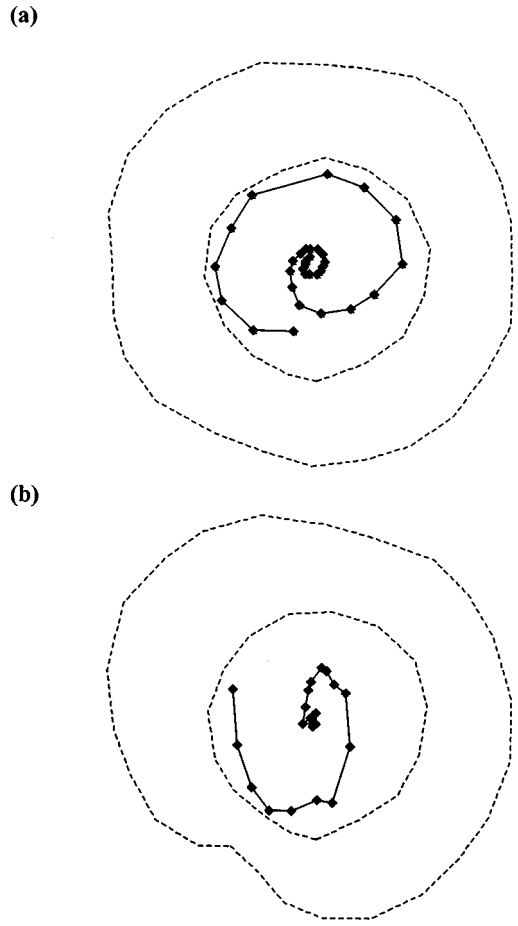

FIG. 5. (a) Trajectory of a single vortex (spiraling inward) after tuning from $q=0$ to 1. Points mark the positions of the vortex at equal time steps. The circular outer boundary represents the ''beam contour'' of the doughnut mode (when the vortex is close to center) and the inner boundary that of the Gaussian before the vortex appears. (b) Outward spiraling trajectory after tuning away from $q=1$.

such as is not encountered with lasers.

III. PERIODIC SWITCHING OF TOPOLOGICAL CHARGE OF VORTEX PAIR (MODE FAMILIES 1 AND 2)

The series of snapshots in Fig. 6 shows the dynamical pattern emitted when the PRO is tuned to between the first- and second-order transverse mode families. The interferograms in Fig. 7 show that the pattern contains two vortices of opposite topological charge, and that these two vortices exchange their topological charge twice each period. A closer look suggests that this pattern contains essentially the Gauss-Hermite modes TEM_{01} and TEM_{20} whose nodal lines are oriented perpendicularly with respect to one another. This orientation is unusual. The appearance of Hermite-shaped patterns suggests some astigmatism of the resonator. However, under such conditions Hermite mode patterns of different order have their black lines oriented along the same direction. The perpendicular orientation of the two constituent mode patterns observed here must then be the consequence of mode competition. Active modes can coexist only when their intensity overlap is smaller than a critical value [2].

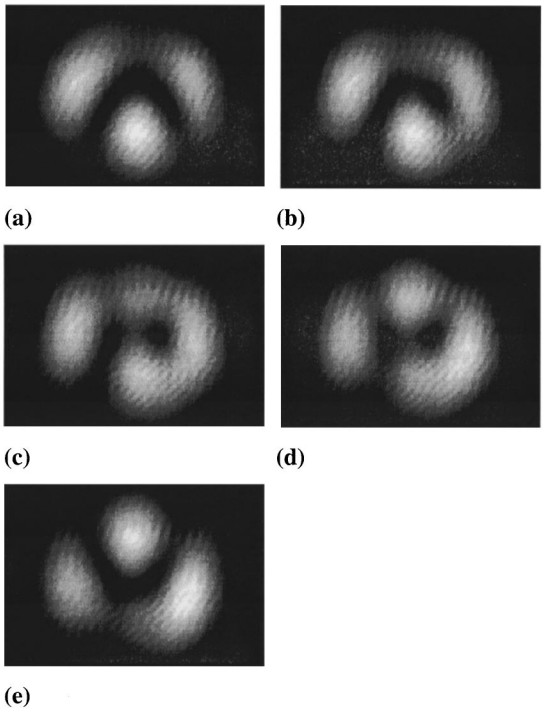

FIG. 6. Video frame sequence showing half of the cycle of the dynamical pattern formed from $q=1$ and 2 mode families. The subsequent half of the cycle reverses the motion with the exception that the helicities of the two vortices are reversed (see Fig. 7).

Here the perpendicular orientation minimizes the overlap.

Figure 8 shows a series of patterns calculated by simple superposition of the Gauss-Hermite mode functions corresponding to TEM_{01} and TEM_{20}:

$$\psi(x,y,t)=[H_{01}(x,y)+e^{i\phi(t)}H_{20}(x,y)]e^{-(x^2+y^2)},$$

where TEM_{01} and TEM_{20} are the Hermite polynomials and $e^{i\phi(t)}$ corresponds to the phase change (linear in time) due to the frequency difference between the two modes. In Fig. 8 $|\Psi|^2$ is plotted since this quantity represents the experimentally observed intensity. The calculated sequence of patterns in Fig. 8 corresponds well to the observed patterns shown in Fig. 6. The phase difference between modes changes by $\pi/4$ between pictures. As shown in Fig. 9, vortices appear at the intersections of the lines along which the real and imaginary part of the optical field is zero ($\mathrm{Re}\{\psi\}$ and $\mathrm{Im}\{\psi\}$ from the above equation equal to zero). In this figure it can be seen how the vortices exchange sign. Figure 9(a) corresponds to the pattern of Fig. 8(c). Here two crossings exist, corresponding to the two vortices. Figures 9(b)(i)–9(b)(iii) correspond to the situation around Fig. 8(a) where there is a dark line of parabolic shape but no vortices. In Figs. 9(a) and 9(b)(iii) the phase differences are slightly smaller and larger, respectively, than in Fig. 9(b)(ii). From these figures, the change of sign of the vortices before and after annihilation, Fig. 9(b)(ii) is apparent.

We have confirmed that this pattern occurs for a laser by a numerical calculation which uses the full partial differential equations of a class-A-laser mode of a PRO [3] instead of a mode description. In the calculation, parameters were used to correspond to the experimental situation. Specifically

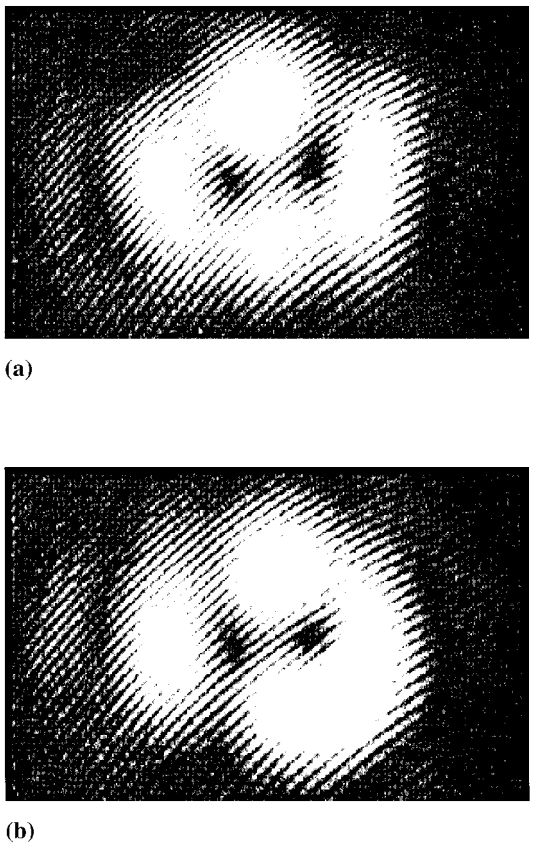

FIG. 7. (a) and (b) Two interferograms from the dynamical pattern depicted in Fig. 6 taken one half cycle apart. The fringe dislocation ''forks'' are pointing away from each other in (a) and toward each other in (b), demonstrating the presence of two oppositely charged vortices which reverse charge every half cycle of the motion.

the parameters chosen were as follows: Gain: 15 times above threshold; mode width of empty resonator (corresponding to the resonator loss, including the linear absorption of the BSO crystal): 0.2 free spectral ranges; tuning: midway between transverse mode families $q=2$ and 3. The introduction of astigmatism was not necessary to make this dynamical pattern appear. This is remarkable. It means that in a perfectly round resonator, where one would expect Gauss-Laguerre modes, Gauss-Hermite modes of rectangular geometry can be emitted due to a spontaneous symmetry breaking.

IV. ROTATING GAUSS-LAGUERRE MODE PATTERN (MODE FAMILY ORDER 3)

The Gauss-Laguerre mode pattern shown in Fig. 10(a) (as a snapshot) is observed near the center frequency of the third-order mode family. This pattern rotates with constant angular velocity as shown in Fig. 10(b). Such a pattern cannot exist in lasers of class A: In an isotropic resonator the ''doughnut'' mode (traveling wave) of higher order, here of order 3, always is favored over the respective Gauss-Laguerre ''flower'' mode (standing wave) [8]. Gauss-Laguerre flower modes can occur only when the resonator anisotropy is seriously perturbed. In this case, however, the pattern could not rotate since rotation requires a very isotropic resonator [9].

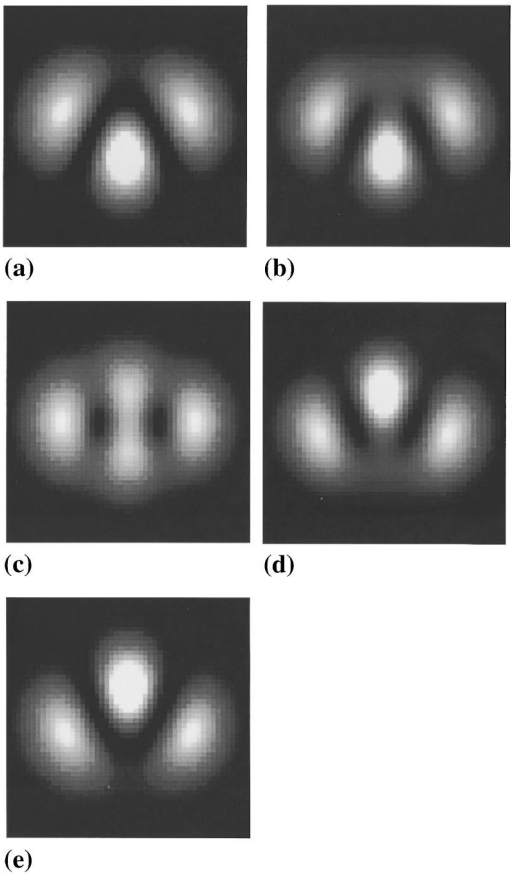

FIG. 8. Calculated intensity, $|\psi(x,y,t)|^2$, showing half of the cycle of the pattern in Fig. 6 formed from a simple superposition of Hermite modes, TEM_{01} and TEM_{20}. The phase difference between the modes changes by $\pi/4$ between each frame.

The occurrence of this rotating Gauss-Laguerre mode pattern must therefore be interpreted in terms of differences between a PRO and a laser. In contrast to a laser, the PRO shows self-focusing, of which some evidence is mentioned above. As was already shown in [8], this nonlinearity can stabilize mode of Gauss-Laguerre flower type even in an isotropic resonator. By analogy with the calculations of [8] where the linewidth enhancement factor (corresponding to self-focusing) was taken into account, one could therefore also expect stable emission of the Gauss-Laguerre flower mode in an isotropic resonator for PRO's, in contrast to lasers. The fact that the flower mode pattern is found to rotate here might be explained by a possible ''helical astigmatism'' of the PRO resonator used. In [11] it has been shown that nonplanar ring resonators, in general, have the property of lifting the frequency degeneracy of right— and left—helical waves. As our ring contains four mirrors, it can be nonplanar and accidental nonplanarity would make the emission frequencies of the two helical fields different, consequently leading to a rotation of the flower mode pattern.

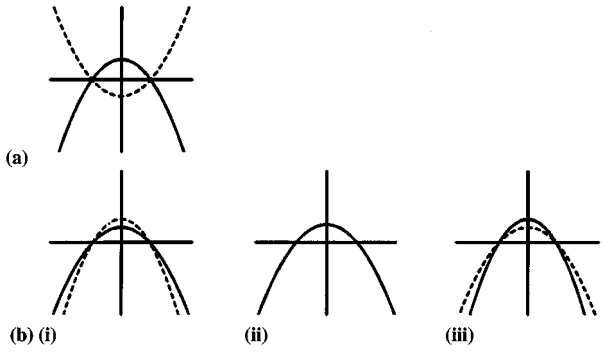

FIG. 9. Zero lines of the real (solid) and imaginary (dashed) parts of the complex field as calculated in Fig. 8 ($\mathrm{Re}\{\psi\}$ and $\mathrm{Im}\{\psi\}$). (a) corresponds to Fig. 8(c), where vortices are clearly present. (b)(i)–(iii) correspond to Fig. 8(a) where vortices annihilate and reappear with exchanged signs.

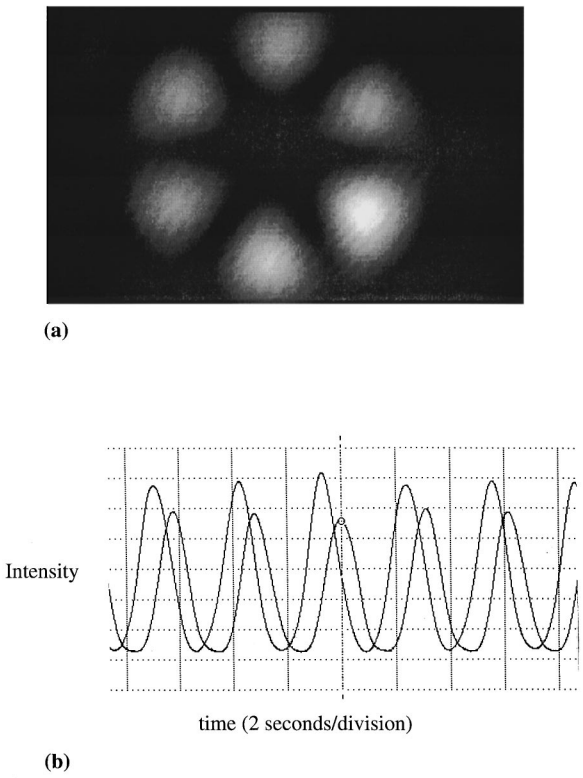

FIG. 10. (a) Single video frame taken from the motion of a circling Gauss-Laguerre $q=3$ mode pattern. (b) Quadrature measurement of the intensity of the pattern as a function of time demonstrating the rotation of the pattern.

V. PULSING TEM_{00} EMISSION

Emission patterns that pulse periodically are frequently observed in the PRO, which are otherwise stationary in class-A lasers. Figure 11 shows two types of pulsing of the simplest type, a periodic and a quasiperiodic pulsing of a TEM_{00} field.

Qualitatively, there are several possible mechanisms for this dynamics. First, it could be understood by considering self-focusing. When the PRO is tuned to TEM_{00} emission, this allows a buildup of the corresponding field distribution in the resonator. The intensity dependence of the material's refractive index will then produce a lens which can put the resonator in the unstable region and, in addition, detunes the resonator. Both effects will prohibit emission. This kind of nonlinearity working here (much in the way as in the application of Kerr-lens mode locking [12]), combined with the

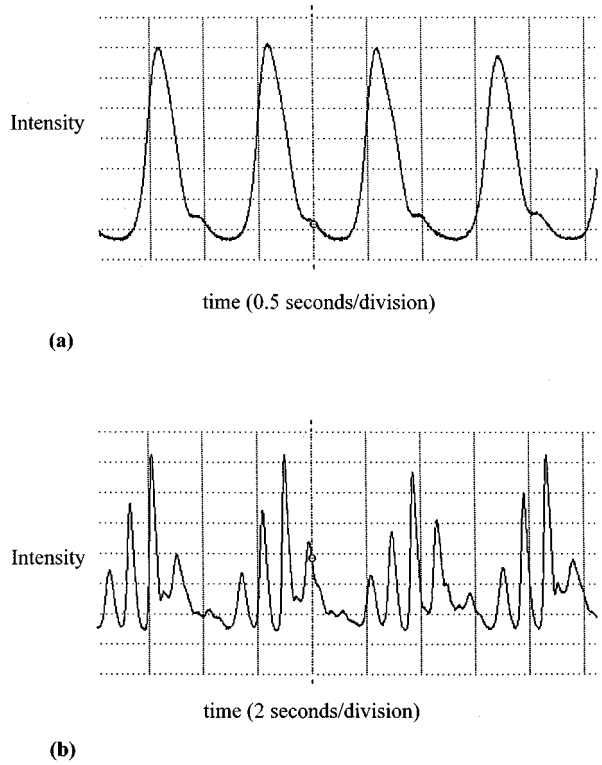

FIG. 11. (a) Regular pulsing of the TEM_{00} Gaussian mode as a function of time. (b) Quasiperiodic pulsing of the same mode. Note that the period in (b) is approximately five times longer.

delay of grating formation in the material, can produce the repetitive pulsing observed. This picture, however, can only be applied to drift-type photorefractive crystals, such as BSO used here, where the beam coupling coefficients contain an imaginary part which leads to self-focusing.

Another possible mechanism for the observed pulsations is intensity-dependent mode pulling [13–15]. The total intensity of the incident light on the photorefractive medium is proportional to the characteristic relaxation time of the medium [14] which is, in turn, inversely proportional to the mode pulling coefficient. Therefore the more intense the radiation in the resonator, the shorter the relaxation time is and the less the mode is pulled to the gain line center. Hence the mode is initially strongly pulled and is consequently well amplified. As the intensity increases, the mode detunes from the gain line center where amplification is then reduced.

Further theoretical studies are required to quantify these mechanisms. Which one of the mechanisms is responsible for the pulsing observed is not clear at the moment. We mention, however, that a numerical calculation using the laser model of [3] of the PRO with parameters, again corresponding to the experiment, and added self-focusing, showed pulsing similar to the experiment. This would indicate that the mechanism producing the pulsing is self-focusing.

In summary, motion of optical vortices and other structures in the field of a PRO have been observed and it is found that they occur largely as is expected for lasers. In particular, the transient spiraling in and out of a vortex gives evidence of the ''particlelike'' or soliton properties of vortices in lasers [7].

However, differences from the dynamics of lasers are also found which can be qualitatively attributed to self-focusing of the photorefractive material. These occur at high pump values. Thus we find that the PRO behaves like a class-A laser, in agreement with what is predicted in [3], close to threshold. In this regime it can be regarded as a ''slow motion laser,' useful to study space-time dynamics of large Fresnel number class-A lasers on a convenient time scale. At higher pump values, differences from a simple class-A laser become apparent, plausibly because here the equivalence with a class-A laser breaks down [3]. Here phenomena more complicated than in simple class-A lasers occur, which seem to allow explanation by additional self-focusing.

Although the PRO, then, is a more complex system than a laser of class A, the additional nonlinearity may produce optical phenomena of interest in nonlinear optics such as solitary waves [10] which would not occur, and hence could not be studied, in lasers.

ACKNOWLEDGMENTS

This work was supported by an ESPRIT BR., ECAUS 001 collaborative grant and Deutsche Forschungsgemeinschaft. J. Malos and M. Vaupel are recipients of a DAAD and Friedrich Naumann-Stiftung-scholarship, respectively.

[1] M. Brambilla, L. A. Lugiato, V. Penna, F. Prati, C. Tamm, and C. O. Weiss, Phys. Rev. A **43**, 5114 (1991).
[2] K. Staliunas, Phys. Rev. A **48**, 1573 (1993).
[3] K. Staliunas, M. F. H. Tarroja, G. Slekys, and C. O. Weiss, Phys. Rev. A **51**, 4140 (1995).
[4] P. Yeh, *Introduction to Photorefractive Non-Linear Optics* (Wiley, New York, 1993).
[5] M. Vaupel and C. O. Weiss, Phys. Rev. A **51**, 4078 (1995).
[6] A. B. Coates, C. O. Weiss, C. Green, E. J. D'Angelo, J. R. Tredicce, M. Brambilla, M. Cattemo, L. A. Lugiato, R. Pirovani, F. Prati, A. J. Kent, and G. L. Oppo, Phys. Rev. A **49**, 1452 (1994).
[7] K. Staliunas, Chaos Solitons Fractals **4**, 1785 (1994).
[8] F. Prati, A. Tesei, L. A. Lugiato, and R. J. Horrowicz, Chaos Solitons Fractals **4**, 1637 (1994).
[9] C. Green, G. B. Mindlin, E. J. D'Angelo, M. G. Solari, and J. R. Tredicce, Phys. Rev. Lett. **65**, 3124 (1990).
[10] M. Vaupel, K. Staliunas, and C. O. Weiss (Phys. Rev. A to be published).
[11] C. Tamm and C. O. Weiss, J. Opt. Soc. Am. B **7**, 1034 (1990).
[12] D. R. Heatley, A. M. Dunlop, and W. J. Firth, Opt. Lett. **18**, 170 (1993).
[13] D. Z. Anderson and R. Saxena, J. Opt. Soc. Am. B **4**, 164 (1987).
[14] G. Alessandro, Phys. Rev. A **46**, 2791 (1992).
[15] L. Dambly and H. Zeghlache, Phys. Rev. A **47**, 2264 (1993).